Interlayer asymmetry gap in the electronic band structure of bilayer graphene

Edward McCann*

PACS 73.63.-b, 73.43.Cd, 81.05.Uw

The low-energy electronic band structure of bilayer graphene consists of four bands: a pair of bands split from zero energy by the interlayer coupling and a pair of bands which touch at zero energy in a nominally undoped system. The latter support massive, chiral quasiparticles with a parabolic dispersion and Berry phase 2π. Asymmetry between the potential energies of the layers opens a tuneable gap between the conduction and valence bands. A self-consistent Hartree approximation is used to model the control of such an interlayer asymmetry gap induced by a transverse electric field in a graphene-based field-effect transistor.

Department of Physics, Lancaster University, Lancaster, LA1 4YB, UK

1 Introduction The discovery that electrons in graphene possess some of the features of relativistic particles has generated huge interest. In monolayer graphene, the low-energy charge carriers are chiral particles exhibiting Berry's phase π with a linear energy-versus-momentum relation [1, 2, 3, 4, 5, 6]. The chirality is based on a 'pseudospin' quantum number arising from the relative phase of the electronic wave function on adjacent atomic sites of the hexagonal lattice and chirality means that the pseudospin always lies parallel or antiparallel to the electron's momentum. The behaviour of low-energy particles in bilayer graphene is perhaps even more remarkable [7, 8, 9]. They have a parabolic dispersion relation and a degree of chirality related to Berry's phase 2π, with the pseudospin linked to, but turning twice as quickly as, the direction of momentum.

It has been possible to describe the electronic band structure of bilayer graphene using both the tight-binding model [10, 7, 11, 12, 13, 14] and density functional theory [15, 16, 17]. It has been predicted [7] that asymmetry between the on-site energies in the layers will create a gap Δ between the conduction and valence bands. As the gap Δ arises from layer asymmetry, there is a possibility of tuning its magnitude using external gates. Indeed, a gate is routinely used in experiments to control the density of electrons n on the bilayer system [1, 2, 8] and, in general, this will produce a simultaneous change in Δ. The dependence of the gap on external gate voltage has been modelled taking into account screening within the tight binding model [13, 14, 17]. It seems that such calculations produce good agreement with ARPES experiments [9], measurements made in the regime of the quantum Hall effect [14], and density functional theory calculations [17].

In the following, we review the tight-binding model of bilayer graphene in Section 2, including trigonal warping effects. We obtain the effective low energy Hamiltonian of bilayer graphene in Section 3 and we show that it is dominated by chiral quasiparticles with a parabolic dispersion and Berry phase 2π. Section 4 describes the opening of a gap in bilayer graphene due to layer asymmetry, followed by a calculation using a self-consistent Hartree approximation to describe the control of the gap in the presence of an external gate.

2 The tight-binding model of bilayer graphene Bilayer graphene consists of two coupled hexagonal lattices with inequivalent sites $A1, B1$ and $A2, B2$ on the bottom and top graphene sheets, respectively,

* Corresponding author: e-mail: ed.mccann@lancaster.ac.uk

arranged according to Bernal ($A2$-$B1$) stacking: as shown in Fig. 1(a), every $B1$ site in the bottom layer lies directly below an $A2$ site in the upper layer, but sites $A1$ and $B2$ do not lie directly below or above a site in the other layer. We use the tight-binding model of graphite [18] by adapting the Slonczewski-Weiss-McClure parameterization [19, 20] of relevant couplings in order to model bilayer graphene. In-plane hopping is parameterized by coupling $\gamma_{A1B1} = \gamma_{A2B2} \equiv \gamma_0$ and it leads to the in-plane velocity $v = (\sqrt{3}/2)a\gamma_0/\hbar$ where a is the lattice constant. We also take into account the strongest inter-layer coupling, $\gamma_{A2B1} \equiv \gamma_1$, between pairs of $A2$-$B1$ orbitals that lie directly below and above each other. Such strong coupling produces dimers from these pairs of $A2$-$B1$ orbitals, leading to the formation of high energy bands [7]. In addition, weaker $A1$-$B2$ coupling $\gamma_{A1B2} \equiv \gamma_3$ is included, leading to an effective velocity $v_3 = (\sqrt{3}/2)a\gamma_3/\hbar$ where $v_3 \ll v$. We write the Hamiltonian [7] near the centers of the valleys in a basis corresponding to wave functions $\Psi = (\psi_{A1}, \psi_{B2}, \psi_{A2}, \psi_{B1})$ in the valley K [21] and of $\Psi = (\psi_{B2}, \psi_{A1}, \psi_{B1}, \psi_{A2})$ in the valley $\tilde{K}$:

$$\mathcal{H} = \xi \begin{pmatrix} -\frac{1}{2}\Delta & v_3\pi & 0 & v\pi^\dagger \\ v_3\pi^\dagger & \frac{1}{2}\Delta & v\pi & 0 \\ 0 & v\pi^\dagger & \frac{1}{2}\Delta & \xi\gamma_1 \\ v\pi & 0 & \xi\gamma_1 & -\frac{1}{2}\Delta \end{pmatrix}, \tag{1}$$

where $\pi = p_x + ip_y$, $\pi^\dagger = p_x - ip_y$, $\mathbf{p} = (p_x, p_y) \equiv p(\cos\phi, \sin\phi)$ is the momentum measured with respect to the K point, $\xi = +1(-1)$ labels valley K ($\tilde{K}$). The Hamiltonian takes into account asymmetry $\Delta = \epsilon_2 - \epsilon_1$ between on-site energies in the two layers, $\epsilon_2 = \frac{1}{2}\Delta$, $\epsilon_1 = -\frac{1}{2}\Delta$.

At zero magnetic field, the Hamiltonian $\mathcal{H}$ has four valley-degenerate bands [7], $\epsilon_\pm^{(\alpha)}(\mathbf{p})$, $\alpha = 1, 2$, with

$$\begin{aligned} \epsilon_\pm^{(\alpha)2} &= \frac{\gamma_1^2}{2} + \frac{\Delta^2}{4} + \left(v^2 + \frac{v_3^2}{2}\right)p^2 + (-1)^\alpha\sqrt{\Gamma} \\ \Gamma &= \tfrac{1}{4}\left(\gamma_1^2 - v_3^2p^2\right)^2 + v^2p^2\left[\gamma_1^2 + \Delta^2 + v_3^2p^2\right] + 2\xi\gamma_1v_3v^2p^3\cos 3\phi. \end{aligned} \tag{2}$$

They are plotted in Fig. 1(b) for $\Delta = 0$ (dashed lines) and $\Delta = \gamma_1$ (solid) where, for simplicity, we neglect v_3. The dispersion $\epsilon_\pm^{(2)}$ describes two bands with energies $\epsilon_+^{(2)} \geq \gamma_1$ and $\epsilon_-^{(2)} \leq \gamma_1$: they do not touch at the K point. These bands are the result of strong interlayer coupling $\gamma_{A2B1} \equiv \gamma_1$ which forms 'dimers' from pairs of $A2$-$B1$ orbitals that lie directly below and above each other [7].

The dispersion $\epsilon_\pm^{(1)}(p)$ describes low energy bands that touch at the K point in the absence of layer asymmetry $\Delta = 0$. In the intermediate energy range, $\frac{1}{4}\gamma_1(v_3/v)^2, |\Delta| < |\epsilon_1| < \gamma_1$, it can be approximated [7] with $\epsilon_\pm^{(1)} \approx \pm\frac{1}{2}\gamma_1[\sqrt{1 + 4v^2p^2/\gamma_1^2} - 1]$. This interpolates between a linear spectrum $|\epsilon_\pm^{(1)}| \approx vp$ at high momenta and a quadratic spectrum $|\epsilon_\pm^{(1)}| \approx p^2/2m$, where $m = \gamma_1/2v^2$. Such a crossover happens at $p \approx \gamma_1/2v$, which corresponds to the carrier density $n^* \approx \gamma_1^2/(4\pi\hbar^2v^2)$. This is lower than the density at which the higher energy band $\epsilon^{(2)}$ becomes occupied $n^{(2)} \approx 2\gamma_1^2/(\pi\hbar^2v^2) \approx 8n^*$. Using experimental graphite values [20] gives $n^* \approx 4.36 \times 10^{12}cm^{-2}$ and $n^{(2)} \approx 3.49 \times 10^{13}cm^{-2}$. The estimated effective mass m is light: $m = \gamma_1/2v^2 \approx 0.054m_e$.

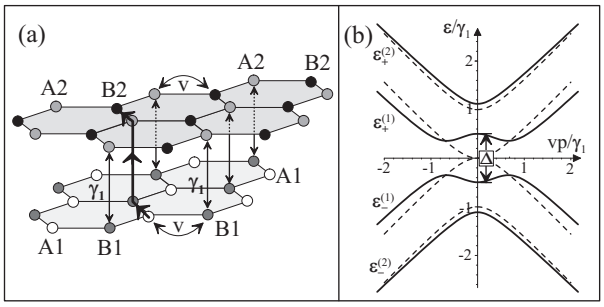

Fig. 1 (a) schematic of the bilayer lattice containing four sites in the unit cell: $A1$ (white circles) and $B1$ (grey) in the bottom layer, and $A2$ (grey) and $B2$ (black) in the top layer. (b) schematic of the low energy bands near the K point obtained by taking into account intralayer hopping with velocity v, $B1A2$ interlayer coupling γ_1, with zero layer asymmetry Δ (dashed lines) and finite layer asymmetry Δ (for illustrative purposes a very large asymmetry $\Delta = \gamma_1$ is used). For simplicity, we neglect $A1B2$ interlayer coupling γ_3.

3 Effective low-energy Hamiltonian The transport properties of bilayer graphene are conveniently described by a low-energy Hamiltonian that describes effective hopping between the non-dimer sites, $A1$-$B2$, *i.e.* those that do not lie directly below or above each other and are not strongly coupled by γ_1. This two component Hamiltonian was derived in [7] using Green's functions. Alternatively (and equivalently), one can view the eigenvalue equation of the four component Hamiltonian Eq. (1) as producing four simultaneous equations for components ψ_{A1}, ψ_{B2}, ψ_{A2}, ψ_{B1}. Eliminating the dimer state components ψ_{A2}, ψ_{B1} by substitution, and treating γ_1 as a large energy, gives the two component Hamiltonian [7] describing effective hopping between the $A1$-$B2$ sites:

$$\begin{aligned} \hat{H}_2 &= -\frac{1}{2m}\begin{pmatrix} 0 & \left(\pi^\dagger\right)^2 \\ \pi^2 & 0 \end{pmatrix} + \hat{h}_w + \hat{h}_a; \qquad (3) \\ \hat{h}_w &= \xi v_3 \begin{pmatrix} 0 & \pi \\ \pi^\dagger & 0 \end{pmatrix}, \quad \text{where} \quad \pi = p_x + ip_y; \\ \hat{h}_a &= -\xi\Delta\left[\tfrac{1}{2}\begin{pmatrix} 1 & 0 \\ 0 & -1 \end{pmatrix} - \frac{v^2}{\gamma_1^2}\begin{pmatrix} \pi^\dagger\pi & 0 \\ 0 & -\pi\pi^\dagger \end{pmatrix}\right]. \end{aligned}$$

The effective Hamiltonian $\hat{H}_2$ is applicable within the energy range $|\epsilon| < \frac{1}{4}\gamma_1$. In the valley K, $\xi = +1$, we determine $\Psi_{\xi=+1} = (\psi_{A1}, \psi_{B2})$, whereas in the valley $\tilde{K}$, $\xi = -1$, the order of components is reversed, $\Psi_{\xi=-1} = (\psi_{B2}, \psi_{A1})$. The Hamiltonian $\hat{H}_2$ describes two possible ways of $A1 \rightleftharpoons B2$ hopping. The first term takes into account $A1 \rightleftharpoons B2$ hopping via the $A2B1$ dimer state. Consider $A1$ to $B2$ hopping as illustrated with the thick solid line in Fig. 1(a). It includes three hops between sites: an intralayer hop from $A1$ to $B1$, followed by an interlayer transition via the dimer state $B1A2$, followed by an intralayer hop from $A2$ to $B2$. Since the two intralayer hops are both A to B, the first term in the Hamiltonian contains π^2 or $(\pi^\dagger)^2$ on the off-diagonal with the mass $m = \gamma_1/2v^2$ reflecting the energetic cost γ_1 of a transition via the dimer state. This term in $\hat{H}_2$ yields a parabolic spectrum $\epsilon = \pm p^2/2m$ with $m = \gamma_1/2v^2$. It has been noticed [7] that quasiparticles described by it are chiral: their plane wave states are eigenstates of an operator $\sigma\mathbf{n}_2$ with $\sigma\mathbf{n}_2 = -1$ for electrons in the conduction band and $\sigma\mathbf{n}_2 = 1$ for the valence band, where $\mathbf{n}_2(\mathbf{p}) = (\cos 2\phi, \sin 2\phi)$ for $\mathbf{p} = (p\cos\phi, p\sin\phi)$. Quasiparticles described by this term acquire a Berry phase 2π upon an adiabatic propagation along a closed orbit, thus charge carriers in a bilayer are Berry phase 2π quasiparticles, in contrast to Berry phase π particles in a monolayer [5].

The second term $\hat{h}_w$ in the Hamiltonian Eq. (3) describes weak direct $A1B2$ coupling, $\gamma_{A1B2} \equiv \gamma_3 \ll \gamma_1$. This coupling $\gamma_{A1B2} \equiv \gamma_3$ leads to the effective velocity $v_3 = (\sqrt{3}/2)a\gamma_3/\hbar$ where $v_3 \ll v$, Eq. (2). In a similar way to bulk graphite [19, 22], the effect of coupling γ_3 is to produce trigonal warping of the isoenergetic lines around each valley. At very low energies $|\epsilon| < \epsilon_L = \frac{1}{4}\gamma_1(v_3/v)^2 \approx 1$meV, the effect of trigonal warping is dramatic. It leads to a Lifshitz transition: the isoenergetic line is broken into four pockets, which can be referred to as one "central" and three "leg" parts [22, 7]. For $v_3 \ll v$, we find [7, 20] that the separation of the 2D Fermi line into four pockets would take place for very small carrier densities $n < n_L \sim (v_3/v)^2\, n^* \sim 1 \times 10^{11} cm^{-2}$. For $n < n_L$, the central part of the Fermi surface is approximately circular with area $\mathcal{A}_c \approx \pi\epsilon^2/(\hbar v_3)^2$, and each leg part is elliptical with area $\mathcal{A}_\ell \approx \frac{1}{3}\mathcal{A}_c$. The overlap between the conduction and valence bands is given by $2\epsilon_L \approx (\gamma_1/2)(v_3/v)^2 \approx 2$meV [12] using $\gamma_1 \approx 0.4$eV and $v_3/v \approx 0.1$. Note that, at energies below the Lifshitz transition, the bilayer spectrum in each of the four Fermi surface pockets is linear, and the integral Berry phase 2π in bilayer graphene [7, 8] is divided into Berry phase π in each of the three side pockets and $-\pi$ in the central one.

4 Voltage-controlled gap in the spectrum of bilayer graphene The parameter Δ takes into account a possibly-externally-controlled asymmetry $\Delta = \epsilon_2 - \epsilon_1$ between on-site energies in the two layers, $\epsilon_2 = \frac{1}{2}\Delta$, $\epsilon_1 = -\frac{1}{2}\Delta$. The electronic bands near the K point, Eq. (2), are shown in Fig. 1(b) for a large value of

the layer asymmetry Δ. For simplicity, we neglect $A1B2$ interlayer coupling γ_3:

$$\epsilon_{\pm}^{(\alpha)2} \approx \frac{\gamma_1^2}{2} + \frac{\Delta^2}{4} + v^2p^2 + (-1)^{\alpha}\sqrt{\frac{\gamma_1^4}{4} + v^2p^2\left(\gamma_1^2 + \Delta^2\right)},$$

The energies of the bands exactly at the K point are $|\epsilon_{\pm}^{(2)}(p=0)| = \sqrt{\gamma_1^2 + \Delta^2/4}$ and $|\epsilon_{\pm}^{(1)}(p=0)| = |\Delta|/2$: the low energy bands, $\epsilon_{\pm}^{(1)}$, are split by the layer asymmetry Δ at the K point [23]. In an asymmetric bilayer, the electronic densities on the individual layers, n_1 and n_2, are given by an integral with respect to momentum $p = \hbar\,|\mathbf{k}|$ over the circularly symmetric Fermi surface, taking into account the relative weight of the wave functions: $n_{1(2)} = (2/\pi\hbar^2)\int p\,dp(\left|\psi_{A1(2)}(p)\right|^2 + \left|\psi_{B1(2)}(p)\right|^2)$, where we have included a factor of four to take into account spin and valley degeneracy. By determining the wavefunction amplitudes on the four separate atomic sites we find

$$n_{1(2)} = \int dp\,p\left(\frac{\epsilon \mp \Delta/2}{\pi\hbar^2\epsilon}\right)\left[\frac{\left(\epsilon^2 - \Delta^2/4\right)^2 \mp 2v^2p^2\epsilon\Delta - v^4p^4}{\left(\epsilon^2 - \Delta^2/4\right)^2 + v^2p^2\Delta^2 - v^4p^4}\right], \tag{4}$$

where the minus (plus) sign is for the first (second) layer.

In the following we use a self-consistent Hartree approximation to determine the electronic distribution on the bilayer and the resulting band structure in the presence of an external gate. We consider the graphene bilayer, with interlayer separation c_0, to be located a distance d from a parallel metallic gate. The application of an external gate voltage $V_g = end/\varepsilon_r'\varepsilon_0$ induces a total excess electronic density $n = n_1 + n_2$ on the bilayer system where n_1 (n_2) is the excess density on the layer closest to (furthest from) the gate (we use SI units). Here ε_0 is the permittivity of free space, ε_r' is the dielectric constant of the material between the gate and the bilayer, and e is the electronic charge. We assume that the screening of the effective charge density $\rho_+ = en$ from the metallic gate is not perfect, leading to an excess electronic density n_2 on the layer furthest from the gate. The excess density n_2 gives rise to an electric field with magnitude $E = en_2/\varepsilon_r\varepsilon_0$ between the layers where ε_r is the nominal dielectric constant of the bilayer. There is a corresponding change in potential energy $\Delta U = e^2n_2c_0/\varepsilon_r\varepsilon_0$ that determines the layer asymmetry [13]:

$$\Delta\,(n) = \epsilon_2 - \epsilon_1 \equiv \frac{e^2n_2c_0}{\varepsilon_r\varepsilon_0}. \tag{5}$$

In terms of the capacitance of a bilayer of area L^2, $C_b = \varepsilon_r\varepsilon_0L^2/c_0$, this may be written $\Delta\,(n) = e^2n_2L^2/C_b$.

We self consistently calculate the excess densities n_1, n_2, $n = n_1 + n_2$, Eq. (4), and the gap Δ, Eq. (5). This has been done numerically in Ref. [13]. Analytically, for moderately low density, $4\pi\hbar^2v^2|n| < \gamma_1^2$, we find

$$\begin{aligned} \Delta &\approx \frac{e^2L^2n}{2C_b}f_{\Lambda}\left(\frac{\hbar^2v^2\pi|n|}{\gamma_1^2}\right), \\ f_{\Lambda}\,(x) &\approx \frac{1}{1 + \Lambda\left(x - \frac{1}{2}\ln x\right)}. \end{aligned} \tag{6}$$

The function $f_{\Lambda}(x)$ depends on the dimensionless parameter $\Lambda = e^2L^2\gamma_1/(2\pi\hbar^2v^2C_b)$ which describes the effectiveness of the interlayer screening of the bilayer. The limit $\Lambda \to 0$ describes poor screening when the density on each layer is equal to $n/2$ whereas for $\Lambda \to \infty$ there is excellent screening, the density lies solely on the layer closest to the external gate and $\Delta = 0$. Note that $f_{\Lambda}(x) \to 0$ as $x \to 0$ because of the logarithm, meaning that the effectiveness of interlayer screening increases upon lowering density. Using typical experimental parameters [20] we find $\Lambda \approx 1.3$. We estimate that the addition of density $n \sim 10^{12}\text{cm}^{-2}$ yields a gap $\Delta \sim 10\text{meV}$ [24].

5 Conclusions We reviewed the results of tight-binding model studies of bilayer graphene and its low-energy electronic band structure. Inter-layer asymmetry creates a gap between the conduction and valence bands so that bilayer graphene is a semiconductor with a tuneable gap of up to about 0.4eV. A self-consistent Hartree approximation was used to determine the density distribution of the two layers when the density n is varied using an asymmetrically placed gate, resulting in a density dependent gap $\Delta(n)$. Control of the gap has been modelled taking into account screening within the tight binding model [13, 14, 17]. It seems that such calculations produce good agreement with ARPES experiments [9], measurements made in the regime of the quantum Hall effect [14], and density functional theory calculations [17]. The use of a single gate modulates the density and the gap simultaneously, but it should be possible to control them independently by employing both a top and a bottom gate. This suggests a route to nanoelectronic devices defined within a single sheet of gated bilayer graphene.

Acknowledgements The author thanks D.S.L. Abergel, V.I. Fal'ko, A.K. Geim, K. Kechedzhi, K. Novoselov, and L.M.K. Vandersypen for useful discussions and EPSRC for financial support.

References

[1] K.S. Novoselov, A.K. Geim, S.V. Morozov, D. Jiang, Y. Zhang, S.V. Dubonos, I.V. Grigorieva, A.A. Firsov, Science **306**, 666 (2004).
[2] K.S. Novoselov, A.K. Geim, S.V. Morozov, D. Jiang, M.I. Katsnelson, I.V. Grigorieva, S.V. Dubonos, and A.A. Firsov, Nature **438**, 197 (2005); Y.B. Zhang, Y.W. Tan, H.L. Stormer, and P. Kim, Nature **438**, 201 (2005).
[3] D. DiVincenzo and E. Mele, Phys. Rev. B **29**, 1685 (1984).
[4] G.W. Semenoff, Phys. Rev. Lett. **53**, 2449 (1984).
[5] F.D.M. Haldane, Phys. Rev. Lett. **61**, 2015 (1988); Y. Zheng and T. Ando, Phys. Rev. B **65**, 245420 (2002); N.M.R. Peres, F. Guinea, and A.H. Castro Neto, Phys. Rev. B **73**, 125411 (2006); A.H. Castro Neto, F. Guinea, and N.M.R. Peres, Phys. Rev. B **73**, 205408 (2006).
[6] T. Ando, T. Nakanishi, and R. Saito, J. Phys. Soc. Japan **67**, 2857 (1998).
[7] E. McCann and V. I. Fal'ko, Phys. Rev. Lett. **96**, 086805 (2006).
[8] K. S. Novoselov, E. McCann, S.V. Morozov, V.I. Fal'ko, M.I. Katsnelson, U. Zeitler, D. Jiang, F. Schedin, and A.K. Geim, Nature Physics **2**, 177 (2006).
[9] T. Ohta, A. Bostwick, T. Seyller, K. Horn, and E. Rotenberg, Science **313**, 951 (2006).
[10] K. Yoshizawa, T. Kato, and T. Yamabe, J. Chem. Phys. **105**, 2099 (1996); T. Yumura and K. Yoshizawa, J. Chem. Phys. **279**, 111 (2002).
[11] C.L. Lu, C.P. Chang, Y.C. Huang, R.B. Chen, and M.L. Lin, Phys. Rev. B **73**, 144427 (2006); J. Nilsson, A.H. Castro Neto, N.M.R. Peres, and F. Guinea, Phys. Rev. B **73**, 214418 (2006); M. Koshino and T. Ando, Phys. Rev. B **73**, 245403 (2006); F. Guinea, A.H. Castro Neto, and N.M.R. Peres, Phys. Rev. B **73**, 245426 (2006); M.I. Katsnelson, Eur. Phys. J. B **51**, 157 (2006); **52**, 151 (2006).
[12] B. Partoens and F. M. Peeters, Phys. Rev. B **74**, 075404 (2006).
[13] E. McCann, Phys. Rev. B **74**, 161403 (2006).
[14] E.V. Castro, K.S. Novoselov, S.V. Morozov, N.M.R. Peres, J.M.B. Lopes dos Santos, J. Nilsson, F. Guinea, A.K. Geim, and A.H. Castro Neto, cond-mat/0611342.
[15] S.B. Trickey, F. Müller-Plathe, G.H.F. Diercksen, and J.C. Boettger, Phys. Rev. B **45**, 4460 (1992).
[16] S. Latil and L. Henrard, Phys. Rev. Lett. **97**, 036803 (2006).
[17] H. Min, B.R. Sahu, S.K. Banerjee, and A.H. MacDonald, Phys. Rev. B **75**, 155115 (2007).
[18] P.R. Wallace, Phys. Rev. **71**, 622 (1947); J.C. Slonczewski and P.R. Weiss, Phys. Rev. **109**, 272 (1958).
[19] M.S. Dresselhaus and G. Dresselhaus, Adv. Phys. **51**, 1 (2002); R.C. Tatar and S. Rabii, Phys. Rev. B **25**, 4126 (1982); J.-C. Charlier, X. Gonze, and J.-P. Michenaud, Phys. Rev. B **43**, 4579 (1991).
[20] We use $\gamma_1 = 0.39eV$ [19, 9], $v_3/v = 0.1$, $v = 8.0 \times 10^5 m/s$ [2], $c_0 = 3.35$Å, and $\varepsilon_r = 1$.
[21] Corners of the hexagonal Brilloin zone are $\mathbf{K}_\xi = \xi(\frac{4}{3}\pi a^{-1}, 0)$, where $\xi = \pm 1$ and a is the lattice constant.
[22] G. Dresselhaus, Phys. Rev. B **10**, 3602 (1974); K. Nakao, J. Phys. Soc. Japan, **40**, 761 (1976); M. Inoue, J. Phys. Soc. Japan, **17**, 808 (1962); O.P. Gupta and P.R. Wallace, Phys. Stat. Sol. B **54**, 53 (1972).
[23] Note that the "mexican hat" structure of the low energy bands means that the true value of the gap $\tilde{\Delta}$ occurs at finite momentum away from the K point. For huge values of the asymmetry $|\Delta| \gg \gamma_1$, the gap would saturate at $\tilde{\Delta} \approx \gamma_1$ although for modest asymmetry values $|\Delta| \ll \gamma_1$, the relation is simply $\tilde{\Delta} \approx |\Delta|$.
[24] In Section 4 we neglected the role of additional weak couplings, such as $A1$-$B2$ coupling γ_3 that results in trigonal warping, Section 3, and is relevant at low density $n \sim 1 \times 10^{11}\text{cm}^{-2}$. Indeed, trigonal warping should result in a small overlap between the conduction and valence band of ≈ 2meV.